Macromolecules

Article

Cite This: Macromolecules 2019, 52, 5480−5490

pubs.acs.org/Macromolecules

Modeling the Influence of Emergent and Self-Limiting Phase Separations among Nascent Oligomers on Polymer Sequences Formed during Irreversible Step-Growth Copolymerizations

Zhongmin Zhang and Kateri H. DuBay*

Department of Chemistry, The University of Virginia, Charlottesville, Virginia, United States

Supporting Information

The sequential ordering of different monomers within synthetic copolymers is remarkably difficult to control. Our understanding of the determinants of and variations within copolymer sequences, even in simple step-growth reactions, remains limited. In this work, we perform simulations on a generic model of irreversible step-growth copolymerization between two types of monomers, A and B, in solution. Our results demonstrate that relatively weak attractions among nascent oligomers can exert considerable influence over the sequential arrangement of monomers in the final set of copolymers, even when identical reaction barriers exist between all monomer pairs. The observed effects cannot be fully accounted for within conventional polymerization theories due to a breakdown in Flory's principle of equal reactivity that occurred in some cases. Nonetheless, these anomalous results can be readily explained by the Flory−Huggins theory, as a phase separation between A-rich and B-rich segments can emerge from and also be limited by the copolymerization process itself. This observation suggests that new routes for the one-pot synthesis of sequence-biased copolymers may be available through the coupling of step-growth copolymerizations and emergent phase separations.

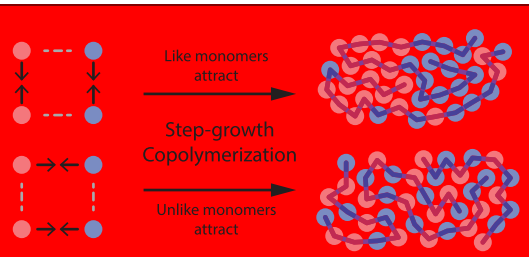

1. INTRODUCTION

Advanced polymers hold great promise for a variety of important applications, ranging from protective coatings on surfaces[1−3] to environmentally responsive materials that can be used for novel memory storage[4−6] and targeted drug delivery.[7−13] The functional properties of a polymer are closely related to its nanoscale morphology, and its nanoscale morphology depends upon its primary structure, that is, its sequence. A crucial limiting factor in optimizing a synthetic polymer's function via the design of its structure is that its sequence is generally not well controlled or even well characterized.[14,15] Significant progress has been made toward the goal of sequence-defined copolymers,[15−19] but these efforts would be enhanced by a better understanding of the determinants of sequence within even standard chain growth and step-growth copolymerizations.

Here, we focus on step-growth copolymerizations. In these reactions, polymerization proceeds via a series of coarsening steps, so that the system is first composed of monomers that react to form dimers, which then react with other monomers or each other to form longer segments, and so on—as opposed to chain-growth polymerizations, wherein monomers add one at a time to the growing chain. Step-growth polymerization reactions are widely used to generate common polymers, particularly, conjugated polymers that can be inaccessible through other synthetic routes, which include donor−acceptor copolymers useful for photovoltaic applications.[20,21] In this work, we seek to better understand the range of factors that can influence the sequences of copolymers formed via an irreversible, solution-based, step-growth reaction.

The reaction kinetics of step-growth homopolymerizations were initially investigated by Flory and Carothers, resulting in standard equations which describe the extent of polymerization and polydispersity.[22] Importantly, Flory found that the reactivity of an end group did not change with the chain length for the reactions studied.[23] Based on generalization of that key result, Mayo and Lewis derived equations that describe how differing monomer-pair rate constants govern reaction kinetics in free radical, chain-growth copolymerizations—specifically how ratios of these rate constants, known as reactivity ratios, govern the relative probabilities of the inclusion of different monomers and the likelihood of different nearest neighbor pairs within the resulting chains.[24,25] According to the standard Mayo−Lewis theory, reactivity ratios remain constant over the course of a single reaction and across reactions with differing monomer feed concentrations.[25] Although this theory was worked out for a chain-growth mechanism, it also provides a useful framework for thinking about step-growth polymerizations. For an irreversible step-growth copolymerization, what ends up bound to what within the chain is still determined by the reaction kinetics between the differing pairs of reactive end groups. Specifically, the reaction rate for each pair of monomers will depend on the

Received: February 6, 2019
Revised: June 4, 2019
Published: July 15, 2019

DOI: 10.1021/acs.macromol.9b00266
Macromolecules 2019, 52, 5480−5490

frequency of collisions between them, the height of their reaction barrier, and the fraction of their collisions that occur with both the correct orientation and sufficient energy to overcome that barrier.

While the fundamental principle of Flory that polymer reactivity does not change with the chain length holds true over an impressively wide range of conditions, it is of course, as Flory himself recognized,[26] an approximation that will break down under certain conditions. How the reaction kinetics of a growing polymer is affected by the formation of an additional polymer bond depends on how the formation of such a bond changes the likelihood of the new reactive end encountering another reactive species with the energy and orientation necessary to form the next bond. In theory, even within simple copolymerization, emergent collective behaviors among the nascent chains, such as chain alignment, self-templating, or phase separations, could significantly influence how often different reactive species encounter one another and the probability of a reaction when they do. Although most of these collective behaviors are not expected to alter reaction barriers heights, their impact on collisions (in terms of frequency, orientation, and energy) could be substantial. As a result, emergent differences in the way that different monomers encounter one another during copolymerization could significantly influence the frequency and placement of those monomers in the resulting copolymer—in ways that would then not be able to be described using ratios of static reaction constants.

A number of studies on radical chain-growth copolymerizations report some of these effects, which are neglected in conventional polymerization theories that rely upon static rate constants. For instance, a "bootstrap" effect has been reported in experiments and simulations and is said to occur when one monomer interacts more or less favorably with the growing copolymer chain than it does with the solvent. In such cases, there could be an emergent increase or decrease in the local concentration of that monomer around the reactive end-group during polymerization, leading to reactivity ratios that shift as a nascent chain grows.[27−29] In addition, copolymerizations between monomers that form prepolymerization aggregates also have been reported to demonstrate deviations from the Mayo−Lewis theory.[30,31] In all these cases, the unconventional behavior is attributed to emergent conditions that differentially influence the collision frequencies of various comonomer pairs.

Such complexities may be expected to exert even more of an influence on the sequences of step-growth copolymers than on those of the chain-growth copolymers described above, but little work has been done, either experimentally or computationally, to investigate how emergent collective behaviors among the growing chains might influence the sequences of these step-growth copolymers. One previous study by Chertovich and co-workers[32] utilized a reactive form of dissipative particle dynamics (DPD) simulations to investigate the influence of nonbonded interactions between two types of monomers on the sequences and structures of copolymers formed via a *reversible* step-growth or interchain exchange process from the melt, which enabled the system to approach its equilibrium distribution of chain sequences and conformations. As a result, macrophase separation occurred, yielding in a system composed mainly of two homopolymers in distinct phases and confirming previous theoretical predictions.[33] However, this study did not address how nonbonded interactions might influence copolymer sequences for *irreversible* step-growth polymerizations, a nonequilibrium process where kinetic effects will be dominant. A later study from the same group simulated an irreversible step-growth copolymerization,[34] but in this case, the polymerization took place in the presence of a striped templating surface in order to determine its influence on sequence and the resulting polymer film morphology. Although the results convincingly demonstrated that a heterogeneous reaction environment could influence the sequences of step-grown copolymers,[34] the study did not consider whether or not such an influential environment could simply emerge during copolymerization as a result of the collective behavior of nascent oligomers.

In this paper, we do so, by investigating the influence of nonbonded interactions on monomer sequences within step-grown copolymers formed in the absence of any external templating. We implement a reactive Langevin Dynamics (LD) simulation of an irreversible step-growth copolymerization between two monomer types, **A** and **B**, in solution, for the case in which any two monomers can react to form a bond. We use a more detailed model of these monomers than in a typical DPD simulation and are thus able to explicitly include steric repulsions, nonbonded attractions, and reaction barriers between our monomers. Using this model, we look at the range of nonbonded interactions and find that even moderate differences in monomer interactions can influence the sequence in a way not predicted by conventional polymer theories.

In Section 2, we outline our model. We then discuss the results we obtain for the polymerization of a homopolymer in Section 3.1 and a variety of heteropolymers in Section 3.2. In Section 3.3, we investigate the kinetic behavior of these copolymerizations, and in Section 3.4, we perform nonreactive simulations of short oligomers of varying lengths to better understand the collective behaviors that emerge as polymerizations proceed. The influence of these emergent behaviors on sequence is investigated in Section 3.5. Finally, in Section 4, we conclude and discuss additional implications of our findings.

2. MODEL

2.1. Monomers with Three Constituent Particles Interact through Both Nonbonded and Bonded Forces.

Our model is composed of a set of interacting coarse-grained spherical beads, each of which represents a single monomer. Although many computational studies of polymerizations have been based on kinetic models,[35] such approaches are not designed for systems where spatial heterogeneities (beyond the terminal and penultimate monomers[35]) influence rates—a particle-based model is necessary to capture such effects. Modeling polymers as interacting beads on a chain has a rich history[36] and continues to be used to explore questions ranging from the role of the chain sequence and stiffness on the equilibrium structures of single chains[37] and bulk polymer morphologies,[38−41] to the role of solvent fluctuations during hydrophobic chain collapse.[42] Within our model, monomers are represented by single beads made up of three particles, as shown in Figure 1a. These constituent particles define the internal structure of each monomer and enable anisotropic interactions, both nonbonded and bonded, between them.

In order to model generalized copolymerization between two types of monomers, each monomer in our system has been given an identity of either **A** (red) or **B** (blue). The interactions between any two monomers then depend on three things: (1) their positions relative to one another, that is,

DOI: 10.1021/acs.macromol.9b00266
Macromolecules 2019, 52, 5480−5490

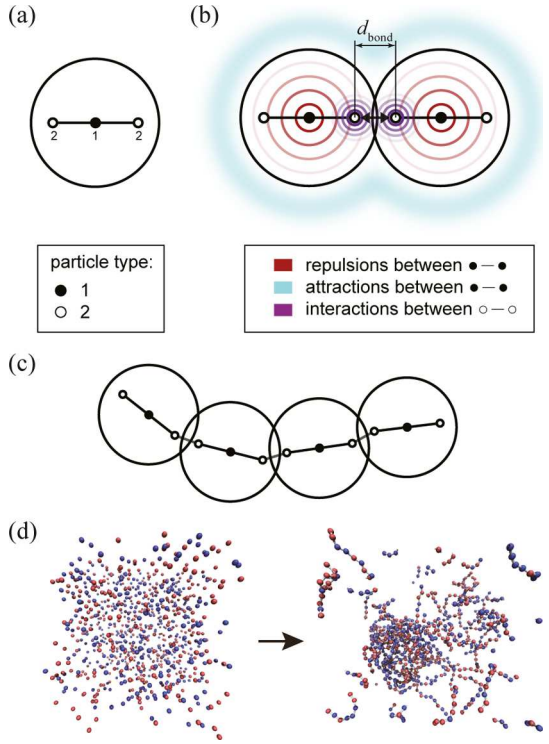

Figure 1. Schematic of the coarse-grained polymerization model. (a) Each monomer is represented by a sphere containing three particles, where the internal distances between type **1** and type **2** particles and the angle between particles **2**−**1**−**2** are restrained by harmonic potentials. (b) Monomers initially interact through nonbonded attractions and repulsions between their type **1** particles as well as through shorter-ranged nonbonded repulsions between their type **2** particles. (c) When type **2** particles on neighboring monomers come within d_{bond} of one another, the interaction between them switches to a harmonic bonded potential, linking the monomers together into growing chains. (d) Thus, as the simulation proceeds, oligomers grow from a collection of randomly distributed unbound monomers.

the distance between them and the relative orientations of their constituent particles; (2) whether or not they are bound to one another; and (3) their identities as either **A** or **B** monomers.

Figure 1b illustrates interactions acting between nonbonded monomers. Attractions and repulsions between the central, type **1**, particles (shown as the solid black circles in Figure 1), are modeled using a Lennard-Jones (LJ) potential that has been modified in such a way that we can independently adjust its repulsive and attractive forces (see Figure S1a), which enables us to make the well depth of the attractive part of the potential dependent on the identities of the interacting monomers (i.e., ϵ_{AA}, ϵ_{BB}, or ϵ_{AB}), while keeping the repulsive forces constant for all monomer pairs. Because we set $\epsilon_{AA} = \epsilon_{BB}$ in this work, we represent this value as $\epsilon_{AA,BB}$. Type **2** particles (shown as the small empty circles in Figure 1) are meant to represent functional groups that react to form the polymer bonds linking monomer units together (see Figure 1c). Interactions between type **2** particles on nonbonded neighboring monomers are designed to introduce a tunable reaction barrier between them (see Figure S1b), while interactions between type **2** particles on bonded neighboring monomers enforce the geometric constraints of the polymer bond, including the bond distance and angles (see Figure S1c).

2.2. Copolymerization Proceeds via Reactive LD. Simulations begin with the monomers randomly distributed, both spatially and orientationally, throughout the simulation box while only nonbonded interactions act between them (see Figure 1d). LD is then used to evolve the system in time, providing a stable temperature over the course of the simulation and the solution-state dynamics appropriate for our coarse-grained monomers in solution.[43]

In order to model the reaction itself, we implemented a coarse-grained reactive dynamics algorithm that makes use of a reaction cutoff distance, d_{bond}, as shown in Figure 1b. The reaction cutoff approach has been used to obtain initial polymer structures for use in a variety of simulations.[44−46] In addition, a coarse-grained reactive molecular dynamics simulation of the polymerization of polystyrene successfully reproduced key results from corresponding atomistic MD simulations.[46] In our implementation, an irreversible harmonic bond forms between two type **2** particles on neighboring unbound monomers whenever they come within d_{bond} of one another. Any two monomers are able to react together and form a bond, so that there is no set sequence predefined by these type **2** reactive groups.

It is important to note that monomers in our simulation must overcome an energy barrier before they get close enough to bind. The energy barrier arises both from repulsions between type **2** particles and from their placement slightly within the minimum of the LJ potential energy function acting between type **1** particles. Because we have separate control over the repulsive and attractive portions of the LJ energy function, the energy barriers can be readily fixed with respect to one another, even when attractions vary.

When the barrier is overcome and a bond is formed, the nonbonded interactions between the bound monomers are turned off and the bonded interactions are turned on. As the simulation proceeds, oligomers form via a step-growth mechanism. In every case, we allow the reaction to proceed until at least 90% of all possible bonds have formed.

2.3. Simulation of Linear Copolymerizations of Small, Solvated Monomers at Room Temperature. The spatial extent of the interactions was chosen to represent a monomer with a diameter of 5 Å, similar to the size of a benzene ring. Relatively weak attractions were introduced between monomers, with the attractive LJ well-depth ranging from 0 to 1.25 k_BT. For comparison, at room temperature, the interaction energy between two parallel benzene rings in a vacuum is about 2.5 k_BT,[47] while the energy of a single, moderate hydrogen bond can range from about 6.7 to 25 k_BT.[48]

Importantly, the initial monomer density is chosen so that the monomers are well dissolved (in the implicit solvent) and miscible. That is, prior to the start of the polymerization reaction, we observe no aggregation and no phase separations among the **A** and **B** monomers, even when the system has been set up with the maximum attractions between all species ($\epsilon_{AA,BB} = \epsilon_{AB} = 1.0\ k_BT$) or the maximum difference in attractions between like and unlike species ($\epsilon_{AA,BB} = 1.25\ k_BT$ and $\epsilon_{AB} = 0\ k_BT$). Because solvent effects are only accounted for in the LD parameters and in the strength of the interactions between monomers, the initial system of monomers is nearly equivalent to a system of simple LJ spheres (differing only in their internal structure, the additional repulsions between type **2** particles and the slightly shifted repulsive portion of the LJ potential). We were therefore able to compare our initial monomer density of $0.058/\sigma^3$ to the gas−liquid phase coexistence density of $0.1/\sigma^3$ estimated from simulations on simple LJ spheres with a k_BT of attraction,[49] thus confirming

DOI: 10.1021/acs.macromol.9b00266
Macromolecules 2019, 52, 5480−5490

that the monomers in our system should reside in the gas region of the phase diagram (which corresponds to a well-dissolved phase in our simulation, given the implicit solvent). See the Supporting Information.

For all combinations of **A** and **B**, the barrier height at the reaction cut-off distance was set to have a contribution of 1.0 k_BT from the LJ interaction between type 1 particles and a contribution of 3.0 k_BT from additional repulsion between type 2 particles. These ideal barriers are what would be encountered if two monomers approached one another with their internal particles at the ideal intramonomer positions and with their binding particles, **1**−**2**−**2′**−**1′**, on a straight line. The actual barriers encountered prior to bond formation vary because they depend on the precise orientations of the pair of binding monomers when they come within d_{bond} of one another. As a result, we monitored the barrier heights at the time of bond formation, observed an average of about 6.5 k_BT, and detected no differences between those encountered by **A** binding to **A**, **A** binding to **B**, and **B** binding to **B**—regardless of how attractive their nonbonded interactions were (see barrier height distributions in Figure S2).

By design, each type **2** particle is only capable of forming one new bond with a neighboring monomer, resulting in linear, unbranched, polymers. In addition, once a polymer bond is formed in our simulation, it cannot be broken. The stiffness of the polymer chain is determined by the potential energy functions governing the angles between the **1**−**2**−**1** and **1**−**2**−**2** particles along the chain. Angular parameters were chosen to be stiff enough so that ring polymer formation of less than 10 monomers is not generally observed but flexible enough to take on a random coil configuration. More detailed information is available in the Supporting Information.

This model was intentionally designed to be as simple as possible while still enabling us to probe the influence of nonbonded interactions on the final sequences for copolymers of typical size, mass, and interaction strengths. In order to consider only the most general set of interactions acting between monomers, we included simple, shorter-ranged, isotropic attractions and repulsions that can collectively account for the effects of sterics, van der Waals forces, and solvation. Using this general set of interactions, we ask if even these ubiquitous intermonomer interactions can influence the resulting sequences.

3. RESULTS AND DISCUSSION

3.1. Random Sequences Form When Intermonomer Attractions Are Identical. To begin, we simulated the growth of a copolymer made up of two types of identical monomers. To do so, we set all attributes of **A** and **B** monomers to be the same, so that we were essentially simulating the growth of a homopolymer, albeit one where, at the beginning, each monomer is labeled **A** or **B**. Maintaining these labels within our code, even when the monomers behave identically, facilitates our analysis and enables a comparison to the cases where the properties of monomers **A** and **B** differ. To conduct these "homopolymer" simulations, we simply set $\epsilon_{AA,BB} = \epsilon_{AB}$. (NB: for all simulations in this paper, the reaction barriers between pairs **AA**, **AB**, and **BB** are set to the same height and the dynamics of monomers **A** and **B** are identical.)

We then explored a range of $\epsilon_{AA,BB,AB}$ values, from 0 k_BT to 1 k_BT. In Figure 2, we display final snapshots, sample sequences, and the likelihood of each monomer in the chain to have a like or an unlike neighbor (all analyzed at reaction extent $p = 0.9$).

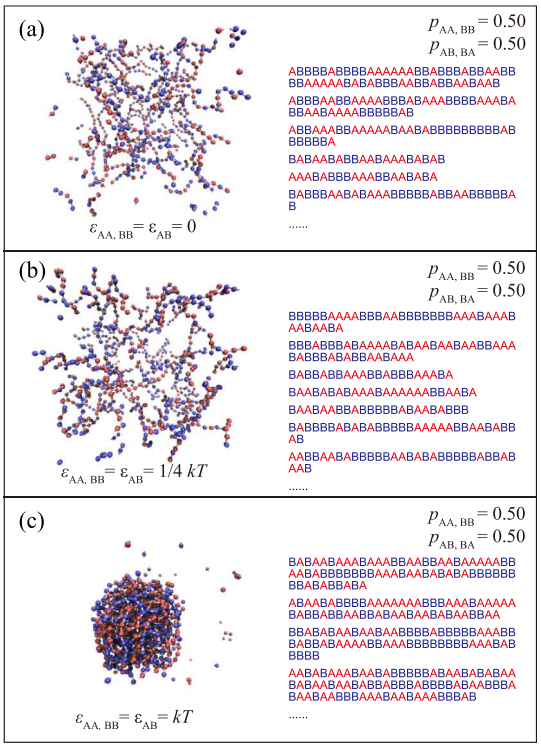

Figure 2. Simulation results when **A** is identical to **B**. Results from a series of polymerizations that started from a uniform distribution of 900 identical monomers, half of which were randomly tagged as **A** (red) and the other half as **B** (blue). On the left, sample final structures of the oligomers resulting from the step-growth simulations (at reaction extent $p = 0.9$) are shown for each case above the ϵ values that governed the strength of the nonbonded LJ attractions. On the right, we show a random sample of the resulting oligomer sequences, as well as the probability of finding a pair of like adjacent monomers ($p_{AA,BB}$) and the corresponding probability of finding a pair of unlike adjacent monomers ($p_{AB,BA}$) within the final set of oligomers. In (a), there are no attractions between nonbonded monomers; in (b), there is 0.25 k_BT of attraction between all nonbonded monomers; and in (c) there is 1.0 k_BT of attraction between all nonbonded monomers. Five simulations were run for each set of ϵ values, and the resulting $p_{AA,BB}$ and $p_{AB,BA}$ values have a standard error of the mean of less than 0.01.

To be precise, the likelihood of like neighbors, $p_{AA,BB}$, is the observed probability of sequential neighbors along the chain (within the set of copolymers obtained at the end of the simulation) having the same identity labels, either **AA** or **BB**. Correspondingly, the likelihood of unlike neighbors, $p_{AB,BA}$, is then the observed probability of sequential neighbors in the simulated copolymers having the opposite identity labels, either **AB** or **BA**.

Our results indicate that, as expected for a system composed of monomers that behave identically, in all cases, there is an even split in the number of nearest neighbor monomer pairs that are tagged with the same identifier (**AA** or **BB**) and those that are tagged with different identifiers (**AB** or **BA**). Thus, the resulting copolymer sequences are completely random, that is, $p_{AA,BB} = p_{AB,BA} = 0.50$ (see Figure 2).

We also observed the phase behavior of oligomers at this homopolymer limit and find that increasing the nonbonded attractions by $\lesssim 1$ k_BT can induce oligomer aggregation. When $\epsilon_{AA,BB} = \epsilon_{AB} = 0$ k_BT (Figure 2a), there are no attractions acting between monomers (although purely repulsive steric

DOI: 10.1021/acs.macromol.9b00266
Macromolecules 2019, 52, 5480−5490

interactions remain), and the resulting oligomers are well dispersed throughout the simulation box. When $\epsilon_{AA,BB} = \epsilon_{AB} = 1/4\ k_BT$ (Figure 2b), oligomers are still well dispersed. However, when $\epsilon_{AA,BB} = \epsilon_{AB} = 1\ k_BT$ (Figure 2c), the oligomers clearly aggregate into a condensed phase.

3.2. Biased Sequences Form When Intermonomer Attractions Differ. We then introduced differences in the intermonomer nonbonded attractions, depending upon the identity of the interacting monomer pair. The reaction barrier heights, sizes, bonded interactions, and nonbonded repulsions were kept constant for all monomer pairs, while the values of $\epsilon_{AA,BB}$ and ϵ_{AB} varied. We investigated several combinations of interactions, ranging from $\epsilon_{AA,BB} = 1\ k_BT$ and $\epsilon_{AB} = 0\ k_BT$ to $\epsilon_{AA,BB} = 0\ k_BT$ and $\epsilon_{AB} = 1\ k_BT$. Simulation snapshots, sample sequences, and the probabilities of like and unlike nearest neighbors are shown in Figure 3 for four of these $\epsilon_{AA,BB} \neq \epsilon_{AB}$ combinations.

When the attractive interactions act between only the like monomers, a bias in the placement of **A** and **B** monomers is observed. With 0.25 k_BT of attraction between like monomers and no attractions between unlike monomers, 58% of nearest neighbor pairs are composed of the same two monomers (Figure 3a), leading to more block-like sequences. Once the attraction between like monomers reaches a full k_BT, the number increases to 89% (Figure 3b). As was observed in the homopolymer case, an attraction of 1 k_BT between like monomers induces oligomer aggregation. However, now that attractions are present between only like monomers, the condensed oligomers also appear to have partially phase-separated into **A**-rich and **B**-rich regions.

When, conversely, the attractive interactions act between only the unlike monomers, another significant bias in the placement of **A** and **B** monomers can be observed, this time toward an alternating sequences. With 0.25 k_BT of attraction between unlike monomers and no attractions between like monomers, 59% of nearest neighbor pairs consist of an **AB** or **BA** pair (Figure 3c), whereas that number again jumps higher, to 78%, once a full k_BT of attraction is present between the unlike monomers (Figure 3d). However, and importantly, at 1 k_BT of attraction, there is no segregation of the **A** and **B** monomers (because they are attracted to one another), and thus, these oligomers do not form dense aggregates observed for the same attraction strength acting between like monomers.

Significant sequence biasing is observed for a variety of $\epsilon_{AA,BB}$ and ϵ_{AB} combinations. Figure 4 shows the probability of having a like nearest neighbor ($p_{AA,BB}$) for a full grid of these attractive values. The purple circles indicate an increased biasing toward unlike neighbors as ϵ_{AB} increases, and the green circles indicate an increased biasing toward like neighbors as $\epsilon_{AA,BB}$ increases. When $\epsilon_{AB} = \epsilon_{AA,BB}$ (on the central diagonal), the probability of like and unlike neighbors is equal. The results in Figure 4 are fairly symmetric around that diagonal, but deviations in this symmetry emerge as the sum of these nonbonded attractions increases and as the strength of the attractions between like monomers increases. The $p_{AA,BB}$ values in the gray and purple points show no trend along each of their diagonals, which means that a composite parameter that is constant along each diagonal, $\Delta\epsilon = \epsilon_{AA,BB} - \epsilon_{AB}$, should be able to fully capture the interaction-dependence of the nearest neighbor probabilities for these points, where attractions between unlike monomers are as strong as, or stronger than, those between like monomers. In contrast, the $p_{AA,BB}$ values along the green diagonals increase with $\epsilon_{AA,BB}$ for the same

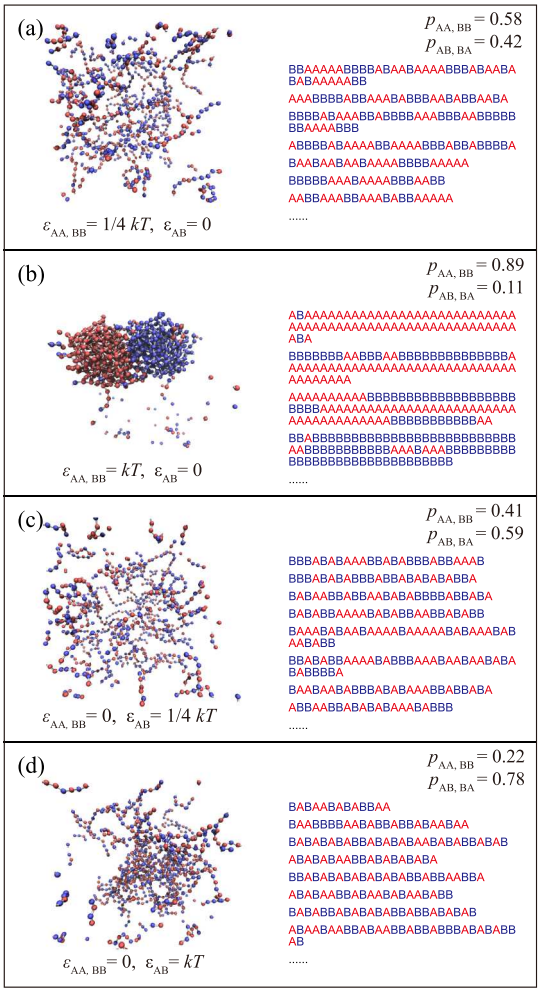

Figure 3. Simulation results when **A** differs from **B**. Results from a series of polymerizations that started from a random mixture of 450 **A** (red) and 450 **B** (blue) monomers. On the left, sample final structures of oligomers (at reaction extent $p = 0.9$) are shown above the ϵ values that governed the strength of the nonbonded LJ attractions. On the right, we show a random sample of the resulting oligomer sequences as well as the values calculated for $p_{AA,BB}$ and $p_{AB,BA}$ within the final set of oligomers. In (a,b), there are no attractions between unlike monomers, with 0.25 k_BT of attraction between like monomers in (a) and a full 1.0 k_BT of attraction between like monomers in (b). In (c,d), there are no attractions between like monomers, with 0.25 k_BT of attraction between unlike monomers in (c) and a full 1.0 k_BT of attraction between unlike monomers in (d). Five simulations were run for each set of ϵ values, and the resulting $p_{AA,BB}$ and $p_{AB,BA}$ values have a standard error of the mean of less than 0.01.

value of $\Delta\epsilon$. This difference in the behavior of the like-attracting monomers and the unlike-attracting monomers can also be seen when comparing the 0.78 value of $p_{AB,BA}$ at $\epsilon_{AB} = 1.0\ k_BT$ and $\epsilon_{AA,BB} = 0.0\ k_BT$ with the significantly higher corresponding 0.89 value of $p_{AA,BB}$ at $\epsilon_{AB} = 0.0\ k_BT$ and $\epsilon_{AA,BB} = 1.0\ k_BT$ (see Figure 3b,d and the upper left and lower right points in Figure 4).

To further probe the resulting oligomer sequences, we also examined the length distributions of blocks of either all-**A** or all-**B** segments within the set of oligomers formed at $p = 0.9$. The results for four $\epsilon_{AA,BB}$ and ϵ_{AB} combinations are shown in Figure 5a. The gray and black histograms show the block length distributions for polymers with the same attractions between like and unlike monomers, the purple histogram

DOI: 10.1021/acs.macromol.9b00266
Macromolecules 2019, 52, 5480−5490

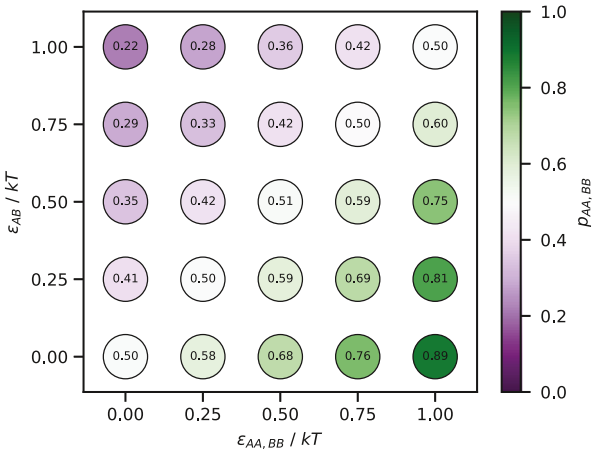

Figure 4. $p_{AA,BB}$ and its dependence on $\epsilon_{AA,BB}$ and ϵ_{AB}. $p_{AA,BB}$, the probability of two adjacent monomers having the same identity, was calculated for 25 different combinations of $\epsilon_{AA,BB}$ and ϵ_{AB} values, which govern the attractions between like and unlike monomers, respectively. The $p_{AA,BB}$ value is shown at each grid-point by a colored circle (see scale bar to the right) with the numerical value at its center. Values were calculated at each point from five independent polymerization runs at a reaction extent of p = 0.9, resulting in a standard error of the mean of less than 0.01 in all cases.

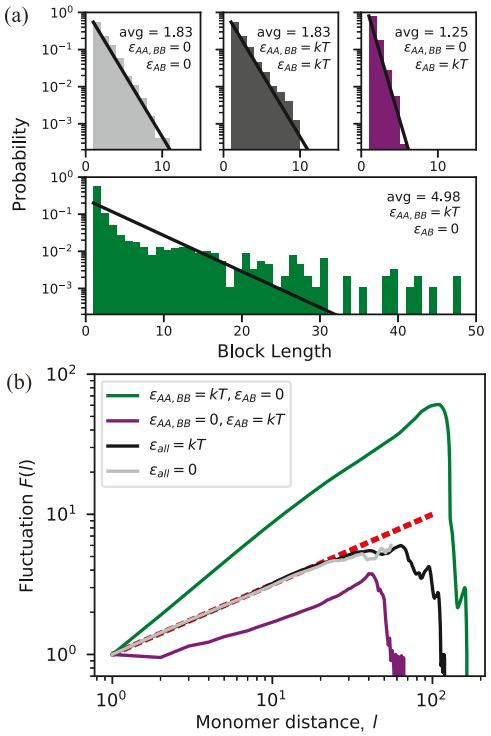

Figure 5. Copolymer sequence analyses. (a) Histograms of block length distributions for polymerized blocks in which all adjacent monomers are the same monomer type were constructed for four combinations of $\epsilon_{AA,BB}$ and ϵ_{AB} values. Using the results from five independent simulations for each case, distributions were constructed for the following cases: no attractions between monomers (light gray, upper left); 1.0 k_BT of attraction between all monomers (black, upper middle); 1.0 k_BT of attraction between only unlike monomers (purple, upper right); and 1.0 k_BT of attraction between only like monomers (green, bottom). Histogram colors were chosen to correspond to the results in Figures 4 and 6. In each case, an ideal distribution (black line) was calculated from the reaction extent, p = 0.9, and the probability, $p_{AA,BB}$, observed for that set of ϵ values (as reported in Figure 4), such that the ideal probability of a block of length n is equal to $(1 - p{\cdot}p_{AA,BB})(p{\cdot}p_{AA,BB})^{n-1}$. (b) Long-range ordering of copolymer sequences examined in part (a) are quantified here by means of the root mean square fluctuation in their accumulated differences in sequential monomer identities, $F(l)$, as a function of the sequential distance, l, between them. The red dashed line shows $F(l) = l^{\alpha}$, where α = 1/2, which is the line expected for a completely random walk in {**A**,**B**} sequence space. For correlated sequences, this random walk scaling behavior with α = 1/2 will only emerge if l is greater than the length scale of the correlation. Additional details on the $F(l)$ calculation are available in the main text.

shows the distribution corresponding to the upper-left point in Figure 4, and the green histogram on the bottom shows the distribution corresponding to the lower-right point in Figure 4.

The average block length is the same for the first two cases. Although there are no attractions between monomers in the first case (Figure 5a, light gray) and 1.0 k_BT of attraction between monomers in the second case (Figure 5a, black), these attractions act between all pairs of monomers. Thus, the **A** and **B** monomers act identically in the simulation, resulting in completely random sequences, for which an average block length of 1.83 monomers was found. When 1.0 k_BT of attraction acts only between unlike monomers (Figure 5a, purple), the chance of having a long block of all one type of monomer decreases, and the average block length is only 1.25 monomers. Finally, for the case when 1.0 k_BT of attraction acts only between like monomers (Figure 5a, green), the chance of having a long block of all one type of monomer increases substantially, and the average block length is 4.98 monomers.

We then sought to determine the consistency of these block length distributions with what would be expected for a Markov chain sequence, that is, where the identity of a monomer in the sequence would depend *only* on the identity of the monomer that immediately precedes it. In our system, statistics consistent with a Markov chain sequence would indicate that there is no long-range biasing of the sequence and, instead, all biasing is due solely to nearest-neighbor effects. An ideal Markov chain block-length distribution for our system can be calculated using the reaction extent, p = 0.9, and the probability, $p_{AA,BB}$, observed for that set of $\epsilon_{AA,BB}$ and ϵ_{AB} values (as reported in Figure 4). Thus, $P_n = (1 - p{\cdot}p_{AA,BB})(p{\cdot}p_{AA,BB})^{n-1}$, where P_n is the probability of an n-length block of all-**A** or all-**B** monomers. In all but the last case, the block-length distributions exactly match the expected Markov chain distributions (Figure 5a, solid black lines) that were calculated for a distribution of sequences with the observed nearest neighbor probabilities from Figure 4. However, in the last case (Figure 5a, green), where ϵ_{AB} = 0.0 k_BT and $\epsilon_{AA,BB}$ = 1.0 k_BT, the block length distribution observed in the simulated copolymers is significantly broader than can be explained by the nearest neighbor probabilities alone, suggesting that longer-range bias has emerged at these values of intermonomeric attractions.

As a way to more precisely quantify the spatial extent of these sequence correlations, we considered the **A**,**B** copolymer sequence as a 1D walk in sequence space, by mapping **A** and **B** monomers to +1 and −1 values, respectively. We then quantified the root mean squared fluctuations of its accumulated differences in sequential monomer identities, $F(l)$, as a function of the sequential distance, l, between them.[50] Specifically, we calculated $F(l) = \sqrt{\langle[\Delta y(l) - \langle\Delta y(l)\rangle]^2\rangle}$, where $\Delta y(l) = y(l_0 + l) -$

DOI: 10.1021/acs.macromol.9b00266
Macromolecules 2019, 52, 5480−5490

$y(l_0)$, l_0 is some initial sequence position along the chain, and l is a sequential distance away from l_0. The net displacement of the walker at sequence position x is $y(x) = \sum_{i=1}^{x} u(i)$, where $u(i)$ is +1 or −1, and i enumerates sequence positions. The angled brackets indicate an average over all possible l_0 positions in a given set of oligomers. For a completely random walk in {**A**,**B**} sequence space, $F(l) \sim l^{\alpha}$, where $\alpha = 1/2$. For correlated sequences, this random walk scaling behavior with $\alpha = 1/2$ will only emerge once l is greater than the length scale of the correlation.

The results of this analysis were plotted in Figure 5b for the same set of intermonomer attractions as in Figure 5a, with the purely random-walk behavior shown as the red dashed line. In the cases where all monomer pairs have the same attraction between them (light gray and black lines), the $F(l)$ line matches the dashed red random-walk line exactly over the full range of l-values for which we have good statistics in our set of oligomers (the $F(l)$ value becomes unreliable after about $l = 30$ because few oligomers grow longer than this length in our simulations). For 1 k_BT of attraction between unlike monomers (purple line), $F(l)$ also displays this characteristic random walk behavior slope of $\alpha = 1/2$, but only after $l = 2$, indicating the presence of a very short-ranged correlation (here, a negative correlation). However, for 1 k_BT of attraction between like monomers (green line), the $F(l)$ line provides clear evidence of long-range ordering[50] that extends beyond the length of the oligomers in our system. These results clearly agree with the block length distribution analysis in Figure 5a. In addition, it is clear that the green line displays correlations that extend far beyond the nearest-neighbor or even the nearest-nearest-neighbor distance in the chain, demonstrating conclusively that even a penultimate kinetic model of polymerization[35] would not be able to capture the extent of these sequence correlations.

3.3. Unconventional Kinetic Features Emerge with Modest Attractions between Like Monomers. To better understand the copolymerization process and the anomalous block length behaviors and sequence correlations in the case where $\epsilon_{AA,BB} = 1.0\ k_BT$ and $\epsilon_{AB} = 0\ k_BT$, we also looked at the degree of polymerization (DoP) and the polydispersity index (PDI) as a function of simulation time. Figure 6a,b show these plots for five $\epsilon_{AA,BB}$ and ϵ_{AB} combinations: three in which attractions act between all monomers (gray scale); one in which $\epsilon_{AA,BB} = 1.0\ k_BT$ and $\epsilon_{AB} = 0\ k_BT$ (green); and one in which $\epsilon_{AA,BB} = 0\ k_BT$ and $\epsilon_{AB} = 1.0\ k_BT$ (purple). Figure 6c displays the PDI at reaction extent $p = 0.9$ for the full set of $\epsilon_{AA,BB}$ and ϵ_{AB} combinations examined in Figure 4.

The number average DoP is $\overline{X}_n = \sum_i N_i X_i / \sum_i N_i$, where the summation runs over i, which indexes different possible chain lengths. X_i is the DoP (or chain length) and N_i is the number of chains of length X_i. Assuming all the polymer chains are linear, the Carothers equation states that $\overline{X}_n = 1/(1 - p)$, where p is the reaction extent.[22] Here, p will be equal to the (number of bonds formed)/(number of all monomers).

The reactions in our simulations should be second order, as two molecules must encounter one another for the reaction to occur. Second-order kinetics has also been experimentally observed for externally catalyzed step-growth polymerizations.[23] According to second-order kinetics and the Carothers equation, the reaction time, t, should be proportional to the number average DoP.[23] In Figure 6a, the polymerizations among monomers with very weak attractions (light gray, dashed gray, and purple curves) do indeed show a linear relationship between DoP and reaction time. However, the polymerizations among monomers with slightly stronger, but still modest, attractions (black and green curves) show a clear nonlinearity and curve upwards (the inset shows this more clearly), indicating that these reactions speed up as they proceed.

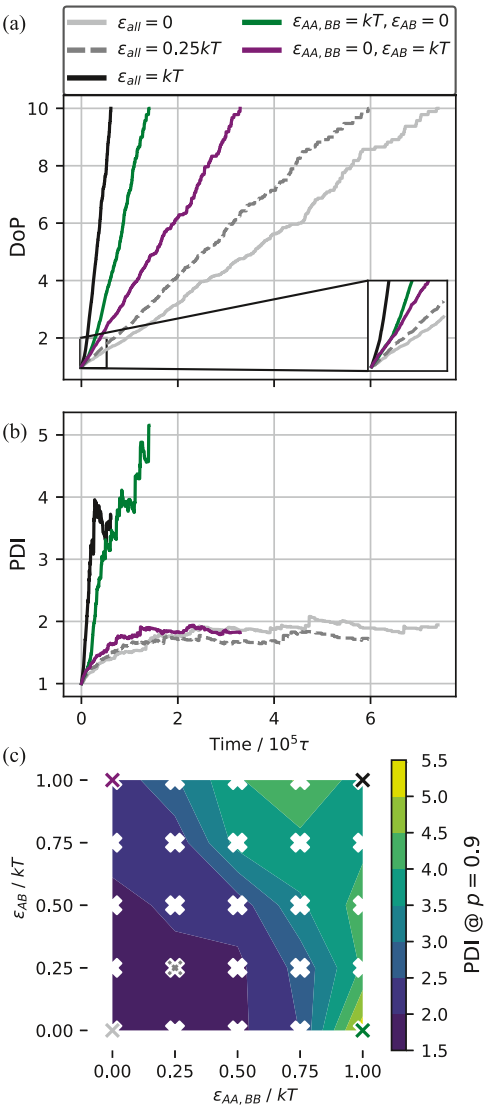

Figure 6. Polymerization kinetics and its dependence on $\epsilon_{AA,BB}$ and ϵ_{AB}. (a) Number average DoP vs reaction time for five combinations of $\epsilon_{AA,BB}$ and ϵ_{AB} values. The gray-to-black lines show the results for increasing attractions between all monomers, the green line shows the case of 1.0 k_BT of attraction between only like monomers, and the purple line shows the case of 1.0 k_BT of attraction between only unlike monomers. (b) PDI vs reaction time for the same set of $\epsilon_{AA,BB}$ and ϵ_{AB} values. (c) PDI at reaction extent $p = 0.9$ is plotted in a color-scale for 25 combinations of $\epsilon_{AA,BB}$ and ϵ_{AB} values, including the five combinations shown in (a,b), which are each marked by a correspondingly colored "X". All data, including kinetic traces, are constructed by averaging over five independent simulations. Isolines in (c) are constructed using linear interpolations along the lines between data points (marked by white "X"s).

The PDI is calculated from PDI = $\overline{X}_w/\overline{X}_n$, where $\overline{X}_w = \sum_i N_i X_i^2 / \sum_i N_i X_i$ is the weight (mass) average. For the ideal chain length distribution, which is expected for systems where reactivity does not change with chain length,[22] the weight average is then $\overline{X}_w = (1 + p)/(1 - p)$, and, using the equations

DOI: 10.1021/acs.macromol.9b00266
Macromolecules 2019, 52, 5480−5490

above, PDI = 1 + p. As a result, in the ideal case, we expect the PDI to reach a plateau at a maximum value of 2 as the reaction proceeds. Again, in Figure 6b, we can see that the polymerizations among monomers with very weak attractions or attractions between only unlike monomers (light gray, dashed gray, and purple curves) display this ideal behavior. However, just as for the DoP, the polymerizations among monomers with modest attractions, on the order of 1 k_BT, between all or like monomers (black and green curves), violate this ideal behavior and climb well above a value of PDI = 2. A PDI larger than two indicates that longer chains preferentially react with other longer chains.

Thus, for monomers with attractions between like monomers on the order of k_BT, we find that: (1) the reactions speed up as polymerization proceeds and (2) longer chains react more frequently with other long chains. Both results are clear indications of a polymerization process that violates Flory's principle of equal reactivity, and therefore cannot be described with a single, static, rate constant.

3.4. Nonreactive Simulations Show That Oligomer Aggregation Depends on Both the Length and $\epsilon_{AA,BB}$. In order to better understand the emergence of these unconventional polymerization behaviors, we performed a series of nonreactive simulations at a fixed density and temperature to look at the phase behavior of a collection of oligomers and explore its dependence on the oligomer length and the attractions between like monomers. The results are shown in Figure 7.

Sets of oligomers were constructed with lengths ranging from 1 to 10 monomers and attractions ranging from $\epsilon_{AA,BB}$ = 0.0−1.25 k_BT (ϵ_{AB} was set to 0). Within each simulation, all oligomers were of the same length, and the **A** and **B** densities were the same as in the reactive simulations. Four different kinds of oligomer sequences were considered: (1) a collection of half all-**A** and half all-**B** homo-oligomers (Figure 7, top left); (2) a collection of identical diblock oligomers made up of two equal-length blocks—one consisting of only **A** monomers, and the other consisting of only **B** monomers (Figure 7, top right); (3) a collection of various sequences that were constructed at random, but are consistent with the $p_{AA,BB}$ probabilities observed for that value of $\epsilon_{AA,BB}$ (Figure 7, bottom left); and (4) a collection of completely randomized sequences (Figure 7, bottom right). Details on oligomer sequence construction are included in the Supporting Information.

The oligomers were placed into the simulation box and then allowed to equilibrate. Qualitatively, the resulting equilibrium oligomer structures were characterized by coding their appearance as either "extended," if they looked well dissolved in the simulation box, "collapsed," if they looked aggregated in the simulation box, or "intermediate," for in between (shown with symbols in Figure 7). Quantitatively, the resulting oligomer structures were characterized by calculating the height of the first peak in the monomer radial distribution function, $g(r)$, which excludes adjacent bound neighbors (shown with the color scale in Figure 7). A small sample of $g(r)$ functions can be seen in Figure S3.

For all interaction strengths, the monomers were well-dispersed in the system and there was no indication of any aggregation in their $g(r)$ functions. However, as the chain lengths increase, and as the interaction strength between like monomers increases, clear evidence of phase separation can be seen for all sequences except the random ones, as indicated by the transition to green and yellow in the top right-hand-corner of each plot in Figure 7. Even the random sequences show some evidence of aggregation at the highest interaction strengths tested.

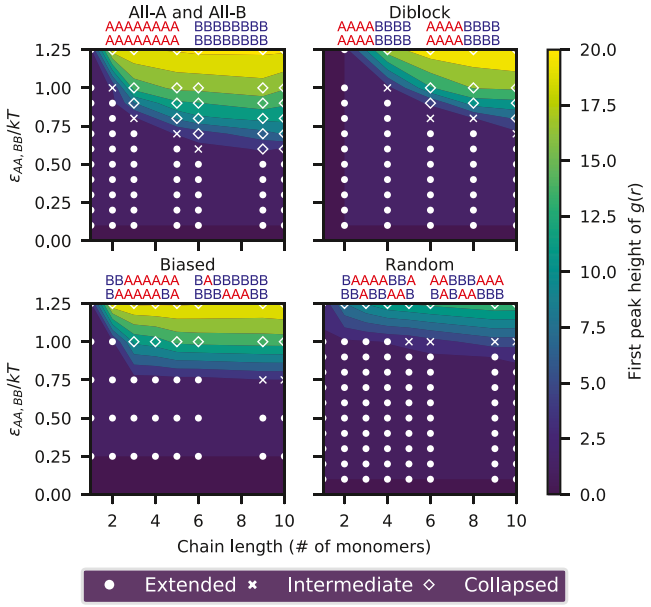

Figure 7. Phase behavior of various oligomers in nonreactive simulations. Equilibrated structures of a collection of nonreactive oligomers with varying sequences and lengths are characterized here by appearance (shown with symbols) and by the height of the first peak in the radial distribution function, $g(r)$, of all monomers (shown with the color-scale). Results are shown for oligomers of different sequences, with four example 8-mer sequences shown at the top of each panel: (top left) a collection of all-**A** and all-**B** homo-oligomers; (top right) a collection of diblock oligomers each consisting of half-**A** and half-**B** monomers; (lower left) a collection of oligomers with randomly chosen sequences in which adjacent monomers on the chain have been biased to conform to the $p_{AA,BB}$ calculated for the corresponding $\epsilon_{AA,BB}$ and ϵ_{AB} values in Figure 4; and (lower right) a collection of oligomers with randomly-chosen sequences with no biasing of the adjacent monomers, such that $p_{AA,BB}$ = 0.5. ϵ_{AB} here is set to 0.0 k_BT in all cases, and oligomers are constructed so that there is a 1:1 ratio of **A** and **B** monomers in each simulation box, with monomer densities comparable to those in the reactive simulations. See the Supporting Information for additional details on oligomer construction. Isolines are constructed using linear interpolations along the lines between datapoints. [NB: The $g(r)$ calculation excludes immediately-bound monomers.]

The reason for the onset of this phase transition as attractions increase is straightforward—stronger attractions favor the condensed phase. The reason for the onset of this phase transition as oligomers lengthen is also clear—the entropic penalty associated with aggregation is reduced once the monomers are connected into chains. Both effects have been well characterized in polymer systems by Flory−Huggins theory,[51] which describes how the phase behavior of a polymer in a solution (or a mixture of two polymers) relates to chain lengths, volume fractions of the different components, and an interaction parameter between them, χ. The complexity in our simulations of having a set of **A**−**B** co-oligomers of different sequences in solution, precludes a quantitative application of Flory−Huggins theory to our system, but the observed trends are as expected.

What this means for our copolymerization is that, as monomers bind together to form ever-lengthening oligomers,

DOI: 10.1021/acs.macromol.9b00266
Macromolecules 2019, 52, 5480−5490

they will begin to phase-separate, with stronger *total* intermonomer attractions spurring aggregation earlier in the polymerization process. This emergent phase separation among the nascent oligomers gives rise to the unconventional polymerization kinetics seen in Figure 6, as the reaction rate increases upon aggregation, leading to a breakdown in applicability of the equal reactivity principle and thus of a static rate constant. In addition, depending on the *difference* in the attraction strengths between like and unlike monomers, the monomer types may also simultaneously phase separate into regions enriched in either **A** or **B**.

3.5. Time Evolution of $p_{AA,BB}$ and Its Partial Dependence on $\Delta\epsilon$. As a result of the insight obtained by the nonreactive simulations, we looked to see if these emergent phase separations actually influence sequence formation by examining the time evolution of $p_{AA,BB}$ during a simulated copolymerization for four different $\epsilon_{AA,BB}$ values (ϵ_{AB} was set to zero). The results are shown in Figure 8. In all cases, there is a high variance in the $p_{AA,BB}$ value during the initial stage of polymerization. After this stage, for the cases of $\epsilon_{AA,BB} = 0\ k_BT$ (gray) and $\epsilon_{AA,BB} = 0.5\ k_BT$ (light green), $p_{AA,BB}$ settles to a value that is *within* the initial variance—to 0.5 for the case of $\epsilon_{AA,BB} = 0\ k_BT$ and to 0.68 for the case of $\epsilon_{AA,BB} = 0.5\ k_BT$. In contrast, for the cases of $\epsilon_{AA,BB} = 1.0\ k_BT$ (green) and $\epsilon_{AA,BB} = 1.25\ k_BT$ (dark green), $p_{AA,BB}$ begins to converge and then jumps up to truly converge at a value that is *above* the range of that initial variance—to 0.89 for the case of $\epsilon_{AA,BB} = 1.0\ k_BT$ and to 0.97 for the case of $\epsilon_{AA,BB} = 1.25\ k_BT$. The latter two results reflect the emergent phase separation among these more attractive monomers as they oligomerize—a phase separation that does, indeed, alter the nearest-neighbor probabilities of the polymer bonds that form after its onset. This effect is the cause of the non-Markovian statistics and long-range correlations observed for the $\epsilon_{AA,BB} = 1.0\ k_BT$, $\epsilon_{AB} = 0\ k_BT$ case in Figure 5. The timescale of this shift to a higher $p_{AA,BB}$ value depends on monomer interaction strength because phase separation will occur among shorter oligomers as $\epsilon_{AA,BB}$ increases in value. Interestingly, the phase separation between **A** and **B** monomers is not complete—in both cases where it occurs, the $p_{AA,BB}$ value converges to a plateau, indicating that this phase separation is limited by the polymer bonds that formed between unlike monomers in the early stage of the copolymerization.

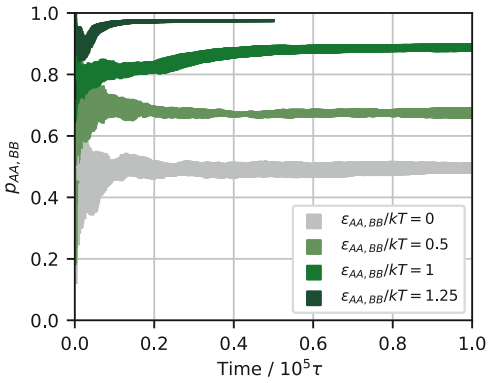

Figure 8. Time evolution of $p_{AA,BB}$ during copolymerization. The value of $p_{AA,BB}$ was monitored during the copolymerization process. Results are reported here for four cases with attractions only between like monomers, varying from $\epsilon_{AA,BB} = 0.0$–$1.25\ k_BT$ ($\epsilon_{AB} = 0.0\ k_BT$). The shaded areas for each trace show the $p_{AA,BB}$ values averaged over ten independent polymerizations, plus and minus one standard deviation.

In order to examine the results of our copolymerization simulations across all the $\epsilon_{AA,BB}$ and ϵ_{AB} combinations tested, we plotted in Figure 9 the final $p_{AA,BB}$ values (at $p = 0.9$) versus $\Delta\epsilon$, while coding each data point by the phase behavior of its oligomers, as quantified by the height of their first $g(r)$ peak. Aggregated oligomer structures are indicated with open diamonds (peak height ≥ 4), while extended coil structures are represented by solid circles (peak height < 4). Sample $g(r)$ functions can be seen in Figure S3. Points along the same diagonal in Figure 4 are shown here in Figure 9 at the same location on the x-axis. A best-fit line was constructed based only on the closed circle points, that is, those that do not undergo a phase transition toward the condensed phase upon polymerization. The $\epsilon_{AA,BB}$ and ϵ_{AB} combinations that lead to an emergent solvent-oligomer phase separation (open diamonds) clearly deviate from this line, but only for the positive values of $\Delta\epsilon$, where like monomers attract. This result clearly demonstrates that the transition to a condensed phase will only influence the sequence if different monomer types are also able to simultaneously undergo a **A**–**B** phase separation, which will only occur if attractions are stronger between like monomers than between unlike monomers (i.e., $\Delta\epsilon > 0$).

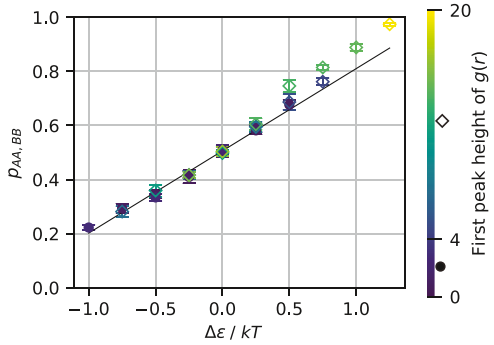

Figure 9. $p_{AA,BB}$ values versus $\Delta\epsilon$. The $p_{AA,BB}$ values shown in Figure 4 (plus one additional case where $\epsilon_{AB} = 0\ k_BT$ and $\epsilon_{AA,BB} = 1.25\ k_BT$) are plotted vs $\Delta\epsilon$, where $\Delta\epsilon = \epsilon_{AA,BB} - \epsilon_{AB}$. Cases where the final set of oligomers are well dissolved (first $g(r)$ peak < 4) are plotted in solid circles, while cases with collapsed aggregates of oligomers (first $g(r)$ peak ≥ 4) are shown in open diamonds. All points are colored by the value of the first $g(r)$ peak height—see the color scale. The set of points represented by the solid circles are used to construct a linear best fit line: $y = 0.30x + 0.51$ and $r^2 = 0.98$. Error bars represent the standard deviations calculated for results that were averaged across five independent polymerization at each point (ten for the $\Delta\epsilon = 1.25\ k_BT$ point).

4. CONCLUSIONS

In this work, we show that even subtle differences in attractions between monomers may influence the "blockiness" of a step-grown copolymer. The influence on the sequence goes beyond what would be expected from additional attractions in an ideal polymerization process, where reactivity does not change with the chain length. Rather, we find that above a relatively weak attraction threshold, a phase separation emerges from and is also limited by the polymerization process itself. This phase separation causes a breakdown of Flory's equal reactivity principle (Figure 6), which can alter the reactivity of certain monomers with other monomers as the polymerization

DOI: 10.1021/acs.macromol.9b00266
Macromolecules 2019, 52, 5480–5490

proceeds (Figure 8). These kinetic effects cannot be described by classical theories that depend on static reaction constants. Our results suggest the possibility of novel synthetic approaches in which relatively slight changes in solvent quality or polymer side chains could be employed to tune interoligomer attractions and thereby influence sequence.

These results are of particular interest in light of recent work to develop polymerization-induced self-assembly (PISA) techniques that yield a desired morphology as a result of polymerization. For instance, in a chain-growth polymerization of amphiphilic diblock copolymers, morphologies ranging from spherical micelles to worms to vesicles can be observed.[52,53] PISA DPD simulations demonstrate that these morphologies are different from equilibrium self-assembly results, suggesting that PISA provides a promising route to interesting non-equilibrium structures.[54] Thus far, the PISA approach involves growing solvophilic monomers on preformed solvophobic oligomers, forming diblock chains. Broadening this concept to include sequence design alongside the morphology design could enable the formation of even more advanced morphologies.

Given the importance of a copolymer's sequence in determining its overall morphology and function, a better understanding of the influence that collective behaviors among nascent chains have on copolymer sequences will enhance our ability to design and to make functionally advanced copolymers.

■ ASSOCIATED CONTENT

Supporting Information

The Supporting Information is available free of charge on the ACS Publications website at DOI: 10.1021/acs.macromol.9b00266.

Additional details are available on the model, the simulations, and the data analysis (PDF).

■ AUTHOR INFORMATION

Corresponding Author

*E-mail: dubay@virginia.edu.

ORCID

Zhongmin Zhang: 0000-0003-3199-6026

Kateri H. DuBay: 0000-0003-3388-1521

Notes

The authors declare no competing financial interest.

■ ACKNOWLEDGMENTS

This material is based upon work supported by the National Science Foundation under grant no. 1848009 as well as a start-up grant from the University of Virginia. The authors would like to thank Kyle Plunkett of Southern Illinois University, Kunlun Hong of Oak Ridge National Lab, Qishen Huang, and Somisetti V. Sambasivarao for many helpful conversations.

■ REFERENCES

(1) Balazs, A. C.; Emrick, T.; Russell, T. P. Nanoparticle polymer composites: where two small worlds meet. *Science* **2006**, *314*, 1107−1110.

(2) Krishnan, S.; Weinman, C. J.; Ober, C. K. Advances in polymers for anti-biofouling surfaces. *J. Mater. Chem.* **2008**, *18*, 3405−3413.

(3) Hanemann, T.; Szabó, D. V. Polymer-Nanoparticle Composites: From Synthesis to Modern Applications. *Materials* **2010**, *3*, 3468−3517.

(4) Ling, Q.-D.; Liaw, D.-J.; Zhu, C.; Chan, D. S.-H.; Kang, E.-T.; Neoh, K.-G. Polymer electronic memories: Materials, devices and mechanisms. *Prog. Polym. Sci.* **2008**, *33*, 917−978.

(5) Church, G. M.; Gao, Y.; Kosuri, S. Next-generation digital information storage in DNA. *Science* **2012**, *337*, 1628.

(6) Bonnet, J.; Subsoontorn, P.; Endy, D. Rewritable digital data storage in live cells via engineered control of recombination directionality. *Proc. Natl. Acad. Sci. U.S.A.* **2012**, *109*, 8884−8889.

(7) Hans, M. L.; Lowman, A. M. Biodegradable nanoparticles for drug delivery and targeting. *Curr. Opin. Solid State Mater. Sci.* **2002**, *6*, 319−327.

(8) Kumari, A.; Yadav, S. K.; Yadav, S. C. Biodegradable polymeric nanoparticles based drug delivery systems. *Colloids Surf., B* **2010**, *75*, 1−18.

(9) Singh, R.; Lillard, J. W. Nanoparticle-based targeted drug delivery. *Exp. Mol. Pathol.* **2009**, *86*, 215−223.

(10) Morachis, J. M.; Mahmoud, E. A.; Almutairi, A. Physical and chemical strategies for therapeutic delivery by using polymeric nanoparticles. *Pharmacol. Rev.* **2012**, *64*, 505−519.

(11) Sankaranarayanan, J.; Mahmoud, E. A.; Kim, G.; Morachis, J. M.; Almutairi, A. Multiresponse strategies to modulate burst degradation and release from nanoparticles. *ACS Nano* **2010**, *4*, 5930−5936.

(12) Fomina, N.; Sankaranarayanan, J.; Almutairi, A. Photochemical mechanisms of light-triggered release from nanocarriers. *Adv. Drug Delivery Rev.* **2012**, *64*, 1005−1020.

(13) de Gracia Lux, C.; Joshi-Barr, S.; Nguyen, T.; Mahmoud, E.; Schopf, E.; Fomina, N.; Almutairi, A. Biocompatible polymeric nanoparticles degrade and release cargo in response to biologically relevant levels of hydrogen peroxide. *J. Am. Chem. Soc.* **2012**, *134*, 15758−15764.

(14) Lutz, J.-F.; Ouchi, M.; Liu, D. R.; Sawamoto, M. Sequence-Controlled Polymers. *Science* **2013**, *341*, 1238149.

(15) Lutz, J.-F. Defining the Field of Sequence-Controlled Polymers. *Macromol. Rapid Commun.* **2017**, *38*, 1700582.

(16) Merrifield, R. B. Solid Phase Peptide Synthesis. I. The Synthesis of a Tetrapeptide. *J. Am. Chem. Soc.* **1963**, *85*, 2149−2154.

(17) Pfeifer, S.; Zarafshani, Z.; Badi, N.; Lutz, J.-F. Liquid-phase synthesis of block copolymers containing sequence-ordered segments. *J. Am. Chem. Soc.* **2009**, *131*, 9195−9197.

(18) Norris, B. N.; Zhang, S.; Campbell, C. M.; Auletta, J. T.; Calvo-Marzal, P.; Hutchison, G. R.; Meyer, T. Y. Sequence matters: Modulating electronic and optical properties of conjugated oligomers via tailored sequence. *Macromolecules* **2013**, *46*, 1384−1392.

(19) Szymański, J. K.; Abul-Haija, Y. M.; Cronin, L. Exploring Strategies To Bias Sequence in Natural and Synthetic Oligomers and Polymers. *Acc. Chem. Res.* **2018**, *51*, 649−658.

(20) Cheng, Y.-J.; Yang, S.-H.; Hsu, C.-S. Synthesis of conjugated polymers for organic solar cell applications. *Chem. Rev.* **2009**, *109*, 5868−5923.

(21) Müllen, K.; Pisula, W. Donor−Acceptor Polymers. *J. Am. Chem. Soc.* **2015**, *137*, 9503−9505.

(22) Carothers, W. H. Polymers and polyfunctionality. *Trans. Faraday Soc.* **1936**, *32*, 39−49.

(23) Flory, P. J. *Principles of Polymer Chemistry*; Cornell University Press, 1953.

(24) Mayo, F. R.; Lewis, F. M. Copolymerization. I. A Basis for Comparing the Behavior of Monomers in Copolymerization; The Copolymerization of Styrene and Methyl Methacrylate. *J. Am. Chem. Soc.* **1944**, *66*, 1594−1601.

(25) Mayo, F. R.; Walling, C. Copolymerization. *Chem. Rev.* **1950**, *46*, 191−287.

(26) Flory, P. J. *Principles of Polymer Chemistry*; Cornell University Press, 1953; pp 77−78.

(27) Harwood, H. J. Structures and compositions of copolymers. *Makromol. Chem., Macromol. Symp.* **1987**, *10-11*, 331−354.

(28) Borisova, O. V.; Zaremski, M. Y.; Borisov, O. V.; Billon, L. The well-defined bootstrap effect in the macroinitiator-mediated pseudo-

DOI: 10.1021/acs.macromol.9b00266
Macromolecules 2019, 52, 5480−5490

living radical copolymerization of styrene and acrylic acid. *Polym. Sci., Ser. B* **2013**, *55*, 573−576.
(29) Gavrilov, A. A.; Chertovich, A. V. Copolymerization of Partly Incompatible Monomers: An Insight from Computer Simulations. *Macromolecules* **2017**, *50*, 4677−4685.
(30) Kazantsev, O. A.; Shirshin, K. V.; Sivokhin, A. P.; Igolkin, A. V.; Goncharova, O. S.; Kamorin, D. M. Copolymerization of sodium 2-acrylamido-2-methylpropane sulfonate with acrylamide and acrylonitrile in water: an effect of conditions on the compositional heterogeneity. *J. Polym. Res.* **2012**, *19* DOI: 10.1007/s10965-012-9886-5.
(31) Kazantsev, O. A.; Kamorin, D. M.; Sivokhin, A. P.; Samodurova, S. I.; Orekhov, D. V.; Korotkova, T. V. Copolymerization of amine-containing monomers and dodecyl (meth)acrylate in toluene: controlling compositional heterogeneity. *J. Polym. Res.* **2014**, *21* DOI: 10.1007/s10965-013-0353-8.
(32) Gavrilov, A. A.; Guseva, D. V.; Kudryavtsev, Y. V.; Khalatur, P. G.; Chertovich, A. V. Simulation of phase separation in melts of reacting multiblock copolymers. *Polym. Sci., Ser. A* **2011**, *53*, 1207−1216.
(33) Semenov, A. N. Secondary super-structures in random copolymers. *Eur. Phys. J. B* **1999**, *10*, 497−507.
(34) Gavrilov, A. A.; Chertovich, A. V. Self-Assembly in Thin Films during Copolymerization on Patterned Surfaces. *Macromolecules* **2013**, *46*, 4684−4690.
(35) Coote, M. L.; Davis, T. P. The mechanism of the propagation step in free-radical copolymerisation. *Prog. Polym. Sci.* **1999**, *24*, 1217−1251.
(36) Groot, R. D.; Warren, P. B. Dissipative particle dynamics: Bridging the gap between atomistic and mesoscopic simulation. *J. Chem. Phys.* **1997**, *107*, 4423−4435.
(37) Hu, D.; Yu, J.; Wong, K.; Bagchi, B.; Rossky, P. J.; Barbara, P. F. Collapse of stiff conjugated polymers with chemical defects into ordered, cylindrical conformations. *Nature* **2000**, *405*, 1030−1033.
(38) Gavrilov, A. A.; Kudryavtsev, Y. V.; Khalatur, P. G.; Chertovich, A. V. Simulation of phase separation in melts of regular and random multiblock copolymers. *Polym. Sci., Ser. A* **2011**, *53*, 827−836.
(39) Gavrilov, A. A.; Kudryavtsev, Y. V.; Khalatur, P. G.; Chertovich, A. V. Microphase separation in regular and random copolymer melts by DPD simulations. *Chem. Phys. Lett.* **2011**, *503*, 277−282.
(40) Song, J.; Shi, T.; Li, Y.; Chen, J.; An, L. Rigidity effect on phase behavior of symmetric ABA triblock copolymers: A Monte Carlo simulation. *J. Chem. Phys.* **2008**, *129*, 054906.
(41) Mao, S.; MacPherson, Q.; Qin, J.; Spakowitz, A. J. Field-theoretic simulations of random copolymers with structural rigidity. *Soft Matter* **2017**, *13*, 2760−2772.
(42) Miller, T. F., 3rd; Vanden-Eijnden, E.; Chandler, D. Solvent coarse-graining and the string method applied to the hydrophobic collapse of a hydrated chain. *Proc. Natl. Acad. Sci. U.S.A.* **2007**, *104*, 14559−14564.
(43) Schneider, T.; Stoll, E. Molecular-dynamics study of a three-dimensional one-component model for distortive phase transitions. *Phys. Rev. B: Condens. Matter Mater. Phys.* **1978**, *17*, 1302.
(44) Duering, E. R.; Kremer, K.; Grest, G. S. Structure and relaxation of end-linked polymer networks. *J. Chem. Phys.* **1994**, *101*, 8169−8192.
(45) Farah, K.; Müller-Plathe, F.; Böhm, M. C. Classical reactive molecular dynamics implementations: State of the art. *ChemPhysChem* **2012**, *13*, 1127−1151.
(46) Farah, K.; Karimi-Varzaneh, H. A.; Müller-Plathe, F.; Böhm, M. C. Reactive molecular dynamics with material-specific coarse-grained potentials: growth of polystyrene chains from styrene monomers. *J. Phys. Chem. B* **2010**, *114*, 13656−13666.
(47) Tsuzuki, S.; Honda, K.; Uchimaru, T.; Mikami, M.; Tanabe, K. Origin of attraction and directionality of the π/π interaction: model chemistry calculations of benzene dimer interaction. *J. Am. Chem. Soc.* **2002**, *124*, 104−112.
(48) Steiner, T. The hydrogen bond in the solid state. *Angew. Chem., Int. Ed.* **2002**, *41*, 48−76.
(49) Watanabe, H.; Ito, N.; Hu, C.-K. Phase diagram and universality of the Lennard-Jones gas-liquid system. *J. Chem. Phys.* **2012**, *136*, 204102.
(50) Peng, C.-K.; Buldyrev, S. V.; Goldberger, A. L.; Havlin, S.; Sciortino, F.; Simons, M.; Stanley, H. E. Long-range correlations in nucleotide sequences. *Nature* **1992**, *356*, 168.
(51) Flory, P. J. *Principles of Polymer Chemistry*; Cornell University Press, 1953; p 495.
(52) Derry, M. J.; Fielding, L. A.; Armes, S. P. Polymerization-induced self-assembly of block copolymer nanoparticles via RAFT non-aqueous dispersion polymerization. *Prog. Polym. Sci.* **2016**, *52*, 1−18.
(53) Warren, N. J.; Armes, S. P. Polymerization-Induced Self-Assembly of Block Copolymer Nano-objects via RAFT Aqueous Dispersion Polymerization. *J. Am. Chem. Soc.* **2014**, *136*, 10174−10185.
(54) Huang, F.; Lv, Y.; Wang, L.; Xu, P.; Lin, J.; Lin, S. An insight into polymerization-induced self-assembly by dissipative particle dynamics simulation. *Soft Matter* **2016**, *12*, 6422−6429.

DOI: 10.1021/acs.macromol.9b00266
Macromolecules 2019, 52, 5480−5490